Development of Fractal-fuzzy Evaluation Methodology and its Application for Seismic Hazards Assessment using Microseismic Monitoring in Coal Mining

Cai, W.

Department of Earth Science and Engineering, Royal School of Mines, Imperial College London, London SW7 2AZ, United Kingdom

School of Mines, China University of Mining and Technology, Xuzhou, Jiangsu 221116, China

Durucan, S., Shi, J.Q., Cao, W., Agrawal, H., Korre, A.

Department of Earth Science and Engineering, Royal School of Mines, Imperial College London, London SW7 2AZ, United Kingdom

Jamnikar, S., Rošer J.

Coal Mine Velenje, Partizanska 78, Velenje, Slovenia

ABSTRACT: Seismic hazards have become one of the common risks in underground coal mining and their assessment is an important component of the safety management. In this study, a methodology, involving nine fractal dimension-based indices and a fuzzy comprehensive evaluation model, has been developed based on the processed real time microseismic data from an underground coal mine, which allows for a better and quantitative evaluation of the likelihood for the seismic hazards. In the fuzzy model, the membership function was built using a Gaussian shape and the weight of each index was determined using the performance metric *F* score derived from the confusion matrix. The assessment results were initially characterised as a probability belonging to each of four risk levels (none, weak, moderate and strong). The comprehensive result was then evaluated by integrating the maximum membership degree principle (MMDP) and the variable fuzzy pattern recognition (VFPR). The model parameters of this methodology were first calibrated using historical microseismic data over a period of seven months at Coal Mine Velenje in Slovenia, and then applied to analyse more recent microseismic monitoring data. The results indicate that the calibrated model was able to assess seismic hazards in the mine.

1. INTRODUCTION

Seismic hazard in mining is the probability of hazard events induced by mining-induced seismicity (Kornowski and Kurzeja, 2012), which have become one of the common risks in underground coal mining and their assessment is an important component of safety management. Such events often include rock bursts and gas outbursts (Li et al., 2007; Ding et al., 2016). With the buildup of these events, the distribution of seismic information, including space, time and energy, are usually seen to be clustering. To capture this clustering phenomenon, the subsurface microseismic monitoring is considered as a potentially powerful tool. The fractal analysis integrated with microseismic monitoring is recognised as a powerful approach towards quantification of the clustering properties.

Since Mandelbrot (1982), who first introduced the use of fractals to describe geometric patterns in nature, it has been widely applied in crustal seismology and earthquake engineering to explain the regional seismicity clustering (e.g. Roy and Gupta, 2015 and references therein), demonstrating that fractal dimension based analysis is an effective method for studying seismic hazards.

Xie and Pariseau (1993) were the first to adopt the fractal dimension to study the rock burst mechanism and evaluate associated seismic hazards in mining. They found that the spatial distribution of seismic events have a fractal clustering structure. The degree of this clustering increases with an approaching main rock burst event which corresponds to a decreasing fractal dimension. This is consistent with the conclusion of a decreasing fractal dimension being associated with the occurrence of a main earthquake in seismology. More recently, further analyses of fractal behaviour of seismic energy (Feng et al., 2016) and time fractal behaviour of seismic events (Yu et al., 2018) confirmed that the distributions of seismic energy and event time also have a fractal structure, as well as the same conclusion that a decreasing fractal dimension is generally an indicator of an approaching rock burst. In

these studies, only a single attribute, i.e. time, space and energy, of seismic information was considered, where the clustering properties were quantified using capacity dimensions.

However, this quantification of seismic clustering of attributes remains at the level of qualitative trend analysis, which can only lead to an indication of such 'abnormal values', without the capability of identifying a certain time period or mining area that is susceptible to a seismic hazard. As Wesseloo (2018) suggested, seismic hazard should be assessed probabilistically, which could then allow one to quantitatively integrate hazard over space and time. In recent years, probabilistic seismic hazard assessment, knowledge-based and data-driven fuzzy modelling, and artificial intelligence methods have been used in a number of studies (e.g. Takuska-Wkgrzyn, 2008; Sun et al., 2009; Kornowski and Kurzeja, 2012; Adoko et al., 2013; Wang et al., 2015; Cai et al., 2016; 2018; Wesseloo, 2018; Afraei et al., 2018; 2019 and references therein).

This paper presents a methodology developed to cover all three aspects of seismic information using real time microseismic monitoring data from an underground coal mine. The developed methodology involves a total of nine fractal dimension-based indices, including both capacity and information dimensions. The latter allows the integration of two or more aspects for an improved quantification of the seismic clustering properties. The methodology was then incorporated into the fuzzy comprehensive evaluation model developed in a previous study (Cai et al., 2018) for the probabilistic and comprehensive assessment of seismic hazards. The application of this methodology has been successfully demonstrated at Coal Mine Velenje in Slovenia.

2. FRACTAL DIMENSION BASED INDICES USING MICROSEISMIC MONITORING DATABASE

2.1. Fractal Dimension Definition
The terms fractal and fractal dimension were coined by Mandelbrot in 1975. It is used to describe geometrical objects which are scale invariant, i.e. the part of an object is similar to the whole, referred to as self-similarity. It has also been used to characterise objects by quantifying their complexity through comparing how detail changes with the scale at which it is measured. These fractal objects have a power-law dependence on the scale and the power is the so-called fractal of Hausdorff dimension D. Consider an assembly of objects which are embedded in a hyper-volume in an E-dimensional Euclidean space with a maximal linear length L. The fractal dimension is usually calculated by covering the objects with hyper-boxes of a linear length ε or a hyper-volume given by ε^{-D_E} ($\varepsilon \leq L$; $D_E \geq D$ is the dimension of the Euclidean

space where the objects are embedded), and counting the number $N(\varepsilon)$ of boxes that contain objects:

$$N(\varepsilon) \propto \varepsilon^{-D} \qquad (1)$$

where the symbol $\propto$ denotes proportionality. This scale rule is typical of conventional rules with respect to the Euclidean geometry and dimensions, which is illustrated in Fig. 1. It is quantified that $D=1$ for lines (1-dimensional objects having length only) because $N(\varepsilon)=3$ when $\varepsilon=1/3$; $D=2$ for surfaces (2-dimensional objects having length and width); $D=3$ for volumes (3-dimensional objects having length, width and height); and a special case $D=0$ for points (0-dimensional objects). When this changes for fractal sets, the non-integer dimension will have a value not equal to the space it resides in.
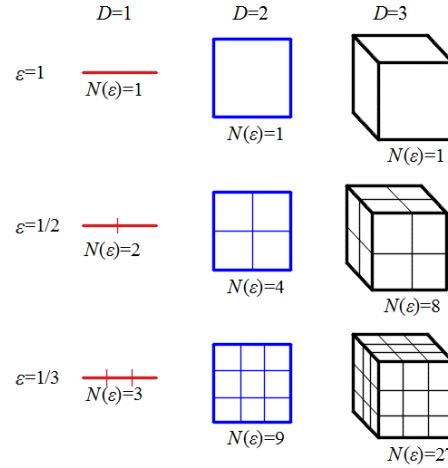

Fig. 1. Traditional notions of the Euclidean geometry for defining scale and dimension.

2.2. Capacity Dimension based Indices
Depending on the characteristics of microseismic data, there are three kinds of calculation scales for the capacity dimension (D_0) to be defined in space (D_{S0}), time (D_{T0}) and energy (D_{E0}). Following Eq. (1), the three scale values of D_0 can be obtained by performing a regression analysis of the plot $logN(\varepsilon)$ vs $log(\varepsilon)$.

$$D_0 = -\lim_{\varepsilon \to 0} \frac{logN(\varepsilon)}{log(\varepsilon)} \qquad (2)$$

In this study, the box-counting method was adopted to estimate $N(\varepsilon)$ corresponding to the three scales. The study areas are first discretised into small 2D boxes of ε in space length (Fig. 2 (a)), 1D line segments of ε in time axis length (Fig. 2 (b)), and 1D line segments of ε in energy axis length (Fig. 2 (c)), respectively. Then a group of data set (ε, $N(\varepsilon)$) is generated through changing the length ε , where $N(\varepsilon)$ is the smallest number of hypothetical boxes which can cover all seismic events, as shade boxes displayed in the figures.

2.3. Information Dimension based Indices
Capacity dimension D_0 mentioned above does not consider the specific information about the number of seismic events or the amount of seismic energy in each

box, and thereby the capacity dimension D_0 might not be the best way to fully extract information of microseismicity in a statistical sense, even though it has been applied for seismic hazards assessment utilising microseismic data. In this context, further statistical extraction should be considered with the assistance of the information dimension D_1, which is based on the normalised probabilities $P_i(\varepsilon)$ for measure in the ith box and defined as:
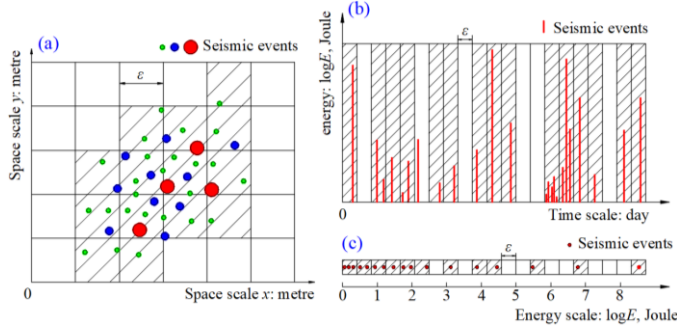

Fig. 2. Box-counting method for estimating fractal dimension in the (a) space scale, (b) time scale, and (c) energy scale of microseismic events. Filled circles indicate seismic events and different colours represent different magnitudes.

$$P_i(\varepsilon) = \frac{m_i}{\sum_{i=1}^{N(\varepsilon)} m_i} \quad (3)$$

$$I_1(\varepsilon) = \sum_{i=1}^{N(\varepsilon)} \{P_i(\varepsilon) \cdot log[P_i(\varepsilon)]\} \quad (4)$$

$$D_1 = -\lim_{\varepsilon \to 0} \frac{I_1(\varepsilon)}{log\varepsilon} = -\lim_{\varepsilon \to 0} \frac{\sum_{i=1}^{N(\varepsilon)} \{P_i(\varepsilon) \cdot log[P_i(\varepsilon)]\}}{log\varepsilon} \quad (5)$$

where $I_1(\varepsilon)$ is the Shannon entropy, m_i is the number of seismic events or the amount of seismic energy in the ith box, and $\sum_{i=1}^{N(\varepsilon)} m_i$ is the total number of seismic events or the total amount of seismic energy. Accordingly, these information dimensions are named as $D_{1\text{-N}}$ and $D_{1\text{-E}}$, respectively. Specifically, the information dimensions, in terms of different time-space-energy scales with box-counting measures, are further divided into $D_{S1\text{-N}}$ and $D_{S1\text{-E}}$ in space scale, $D_{T1\text{-N}}$ and $D_{T1\text{-E}}$ in time scale, and $D_{E1\text{-N}}$ and $D_{E1\text{-E}}$ in energy scale.

In this study, capacity and information dimension based indices were both selected as inputs, although the information dimensions will be more effective than mere extraction of capacity dimension for the assessment of seismic hazards. They include three capacity dimension indices (D_{S0}, D_{T0} and D_{E0}) and six information dimension indices ($D_{S1\text{-N}}$, $D_{S1\text{-E}}$, $D_{T1\text{-N}}$, $D_{T1\text{-E}}$, $D_{E1\text{-N}}$ and $D_{E1\text{-E}}$).

3. A FRACTAL-FUZZY EVALUATION METHODOLOGY FOR SEISMIC HAZARDS ASSESSMENT

Based on the fuzzy comprehensive evaluation model developed in a previous study (Cai et al., 2018), a fractal-fuzzy evaluation model for seismic hazards assessment was developed using the fractal dimension based indices as inputs, which includes three key sections to determine: the membership function for each fractal dimension based index, the weight for each index, and the probabilistic and comprehensive assessment for seismic hazards. More specifically, there are six key steps as illustrated in Fig. 3 and summarised below:
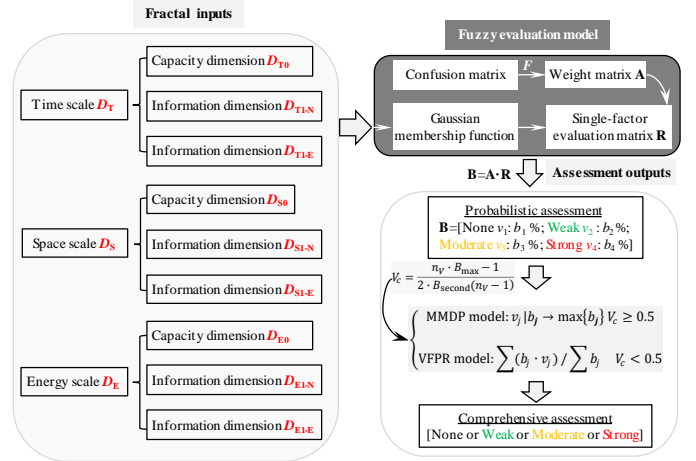

Fig. 3. Framework of the fractal-fuzzy evaluation methodology for seismic hazards assessment using microseismic data.

- Build the factor set $\mathbf{W} = \{D_{T0}, D_{T1-N}, D_{T1-E}, D_{S0}, D_{S1-N}, D_{S1-E}, D_{E0}, D_{E1-N}, D_{E1-E}\}$.
- Build the alternative set $\mathbf{V} = \{v_1, v_2, v_3, v_4\} = \{none, weak, moderate, strong\}$.
- Build the single-factor evaluation matrix $\mathbf{R}$ (see Eq. (6), here $q=9$) using a Gaussian membership function. The component r_{ij} in this matrix $\mathbf{R}$ means the membership degree of the ith factor to the jth alternative subset.

$$\mathbf{R} = \begin{bmatrix} r_{11} & r_{12} & r_{13} & r_{14} \\ r_{21} & r_{22} & r_{23} & r_{24} \\ ... & ... & ... & ... \\ r_{q1} & r_{q2} & r_{q3} & r_{q4} \end{bmatrix} \quad (6)$$

- Determine the weight set $\mathbf{A} = \{a_1, a_2, ..., a_9\}$ using the performance metric F score derived from the confusion matrix.
- Determine the probabilistic assessment for each risk level $\mathbf{B} = \mathbf{A} \cdot \mathbf{R} = \{b_1, b_2, b_3, b_4\}$.
- Locate the comprehensive assessment combining with the maximum membership degree principle (MMDP) and the variable fuzzy pattern recognition (VFPR).

3.1. Membership Function of each Fractal Dimension based Index

Microfracturing and associated dynamic instability in rocks can occur at different scales (Scholz, 1968; Alber et al., 2009; Amitrano, 2012; Qian, 2014; Cheng et al., 2017), e.g., acoustic emission (AE) from coal/rock specimen failure in the laboratory, microseismicity from rock bursts in the underground mines, and seismicity corresponding to the landslide and earthquake in the

crustal field. Therefore, AE measurements during laboratory tests of coal samples to failure can provide a useful guidance on the determination of microseismicity indicators for seismic hazards assessment.

Based on the curves of stress and AE performances verse strain created from the loading test of a typical coal sample, as displayed in Fig. 4, five phases are observed: compaction (OA), elastic deformation (AB), stable microcrack growth (BC), unstable microcrack propagation and macro-fracture formation (CD), and post-failure (DE). During the stable phase BC, AE events increase significantly, as well as the associated fractal indices. After approaching the point C, the fractal dimensions first decrease for a while and then increase to the high value again, and finally drop dramatically until the failure (point D) occurs. It should be noted that this same evolution can be also obtained from the information dimension indices, although only the capacity dimensions are presented here. In this context, it can be concluded that the macro-fractures are formed by joining of microcracks and then cause the final failure. In response to this process from microcrack growth and propagation to macro-fracture formation (around C) and finally to the failure occurrence (around D), there will be a precursor within low value anomaly in fractal dimension indices calculated on the basis of AE monitoring data. Therefore, this precursor can be used for the failure assessment. Accordingly, an anomaly index A_D, which is based on fractal dimensions for categorising seismic hazard levels, can be defined by referring to the definition of b-value anomaly (Mutke et al., 2016):

$$A_D = \frac{D_b - D}{D_b} \tag{7}$$

where D is the fractal dimension index, calculated in a given time window, and D_b is the background value of D, determined using the entire catalog of seismic events previously recorded during coal mining.
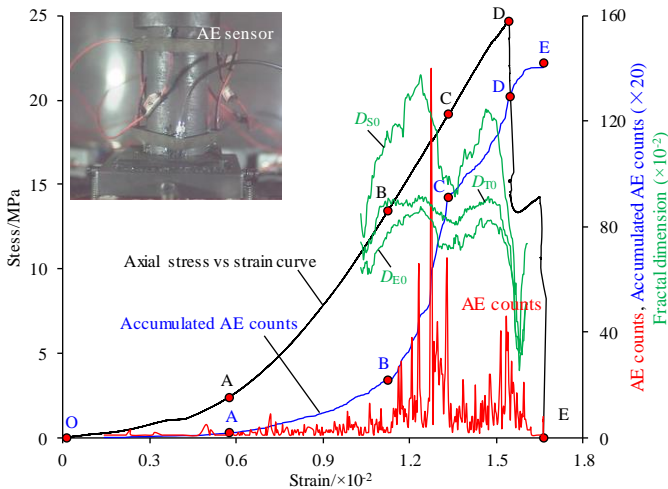

Fig. 4. Evolution of fractal dimensions on AE performances in response to a coal sample under loading to failure.

Building upon Eq. (7), four risk levels (none, weak, moderate and strong) are suggested in this work to categorise seismic hazards, which correspond to the anomaly index value ranges (0 to 0.25, 0.25 to 0.50, 0.50 to 0.75, and 0.75 to 1).These four levels constitute the alternative set $\mathbf{V} = \{\text{none, weak, moderate, strong}\}$ in the fuzzy set theory. On this basis, a Gaussian shape membership function is built as displayed in Fig. 5:
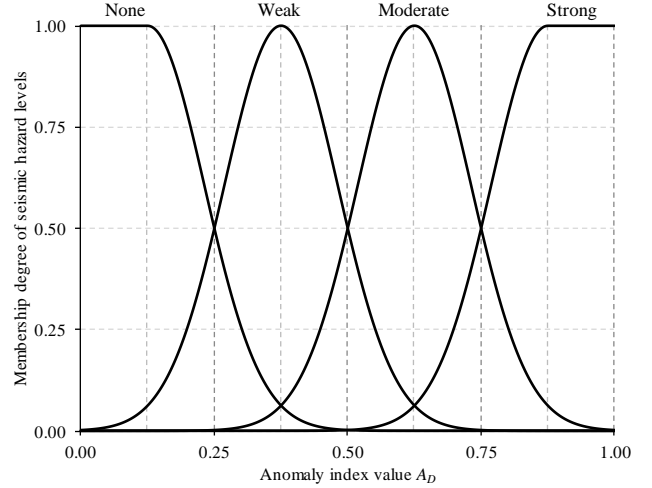

Fig. 5. Gaussian shape membership function based on the anomaly index A_D for categorising seismic hazard levels.

3.2. Weighting of each Fractal Dimension based Index

Seismic hazards assessment can be considered as a two-class prediction problem (Li and Jimenez, 2018), so that there are four possible situations, which constitute the confusion matrix (Fawcett, 2006):

- True positive (TP): the actual condition (hazard forms) and the prediction are both positive.
- False negative (FN): the actual condition (hazard forms) is positive but the prediction is negative.
- True Negative (TN): the actual condition (no hazard forms) and the prediction are both negative.
- False Positive (FP): the actual condition (no hazard forms) is negative but the prediction is positive.

Based on these four situations, the F score was adopted in this study to evaluate the assessment accuracy of each fractal dimension index for seismic hazards. It is defined as (Fawcett, 2006):

$$F = \frac{2 \cdot TP}{2 \cdot TP + FN + FP} \tag{8}$$

In calculation, the risk levels (weak, moderate and strong) need to be considered to classify each index in assessing potential seismic hazards, respectively, and their values of F score are signified as F_W, F_M and F_S accordingly. The overall assessment score is calculated by assigning different weightings to the individual F values corresponding to different risk levels:

$$F_{i\text{com}} = \frac{0.75 \cdot F_S + 0.50 \cdot F_M + 0.25 \cdot F_W}{0.75 + 0.50 + 0.25} \tag{9}$$

The weight of each index can then be calculated by the following normalisation:

$$a_i = \frac{F_{i\text{com}}}{\sum F_{i\text{com}}} \tag{10}$$

3.3. Probabilistic and Comprehensive Assessment of Seismic Hazards

As illustrated in Fig. 3, the probabilistic assessment for the degree of each hazard level can be determined by **B**=**A**·**R**= {None v_1: b_1%; Weak v_2: b_2%; Moderate v_3: b_3%; Strong v_4: b_4%} .

With respect to the comprehensive assessment of seismic hazards, the commonly-used method MMDP considers the maximum membership degree only, which may often make the evaluation result to be uncertain and even fail under some special circumstances, since it ignores the information of other membership degrees. In the current application, an index V_c is defined to check the validity of MMDP:

$$V_c = \frac{n_V \cdot B_{\max} - 1}{2 \cdot B_{\text{second}}(n_V - 1)} \tag{11}$$

where n_V=4 is the number of the alternative subsets in the set **V**. $B_{\max} = \max\{b_i\}$. $B_{\text{second}} = \max_{j \neq i}\{b_j\}$. This index is often applied as:

- When $\boldsymbol{V_c} = +\infty$, MMDP is completely valid.
- When $1 \leq V_c < +\infty$, MMDP is very valid.
- When $0.5 \leq V_c < 1$, MMDP is valid.
- When $0 < V_c < 0.5$, MMDP is invalid.
- When $V_c = 0$, MMDP is completely invalid.

On this basis, the results of MMDP are accepted only for the valid cases. For the rest of invalid cases, the level characteristic value derived from VFPR model is adopted to evaluate the comprehensive result. Therefore, the combination model MMDP-VFPR is established as:

$$V_{\text{index}} = \begin{cases} \text{MMDP model: } v_j | b_j \to \max\{b_j\} & V_c \geq 0.5 \\ \text{VFPR model: } \sum(b_j \cdot v_j) / \sum b_j & V_c < 0.5 \end{cases} \tag{12}$$

where j=1, 2, 3, 4. v_1=0.125, v_2=0.375, v_3=0.625 and v_4=0.875 in the set **V** were designed for numeralisation, in line with the four hazard levels, which correspond to the index value ranges (0 to 0.25, 0.25 to 0.50, 0.50 to 0.75, and 0.75 to 1).

4. FRACTAL-FUZZY EVALUATION MODEL CALIBRATION AND APPLICATION AT COAL MINE VELENJE

4.1. Field Site and Microseismic Monitoring

Located in Slovenia, Coal Mine Velenje currently produces around 3.4 million tonnes of lignite per annum from a lens-shaped deposit, which is up to 165 m thick at the centre and pinches out towards the margins (Fig. 6).

Depth of the seam varies from 200 to 500 m. The mining method used at Coal Mine Velenje is a combination of multi-level mining and longwall top coal caving (LTCC), developed over the decades as the most effective method due to extreme seam thickness, depth and prevailing geotechnical conditions. From the top to the bottom, the entire coal deposit is divided into a series of mining levels ranging from 10 to 20 m thick, mined in time-sequence with at least six months between the mining of each underlying longwall panel. At each level, the lower part of the panel, which is 3 to 4 metres high, is cut by a shearer under the hydraulic supports while the upper section is allowed to cave and be recovered in front of the supports.
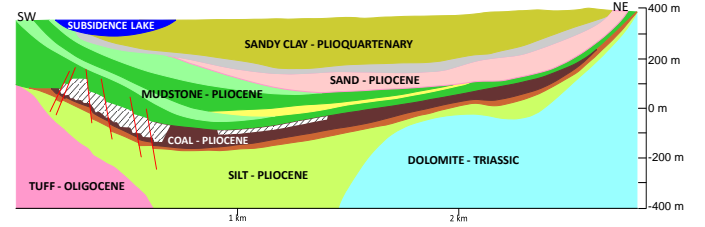

Fig. 6. Schematic SW–NE trending geological cross-section of the Velenje lignite deposit (after Markič and Sachsenhofer, 2010).

Rock bursts and coal/gas outbursts have affected coal production at Coal Mine Velenje since the early days of mine production. Rock burst potential is mostly a concern during development in large coal blocks at the mine. To address this risk, a 32-channel flameproof automated seismic observation system (SOS) developed by the Laboratory of Mining Geophysics of Central Mining Institute (GIG) in Poland was used for real time microseismic monitoring at the mine. For further details of the monitoring systems used, please refer to Si et al. (2015). Microseismic data recorded were collected automatically and transferred to surface data loggers, and then processed to obtain source parameters and event locations. An example of the spatial distribution of two months' recorded microseismic events and the layout of microseismic sensors installed at Coal Mine Velenje are displayed in Fig. 7.

The microseismic monitoring campaign targeted LTCC panels operating at -80 m and -95 m production levels from 2016 onwards. Longwall panels K.-80/B, K.-80/C, K.-80/D, K.-80/E, and CD2 were scheduled to mine during 2016-18 with longwall panels K.-95/A, K.-95/E, K.-95/D and CD3G coming into production during 2018-19 as the -80 m level is being mined-out. It was also recognised that a relatively high stress concentration on areas around the central coal pillar, which protects the main infrastructure in the production district, could increase the risk of seismic hazards in this region considerably, particularly during the development of longwall headings.
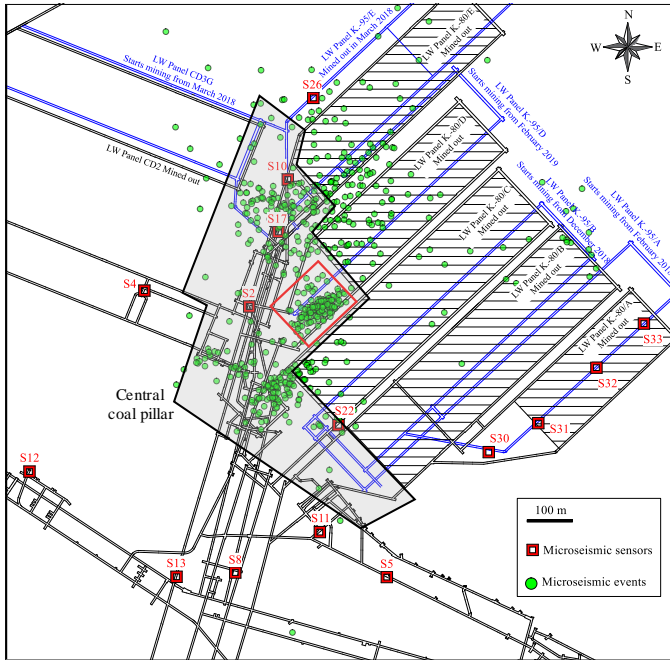
Fig. 7. Longwall layout at -80 and -95 m production levels, production schedule, microseismic sensors installed and the spatial distribution of seismic events occurred during the period 18/02/2018 to 18/04/2018 when longwall panel K.-95/D gateroad was being driven at Coal Mine Velenje.
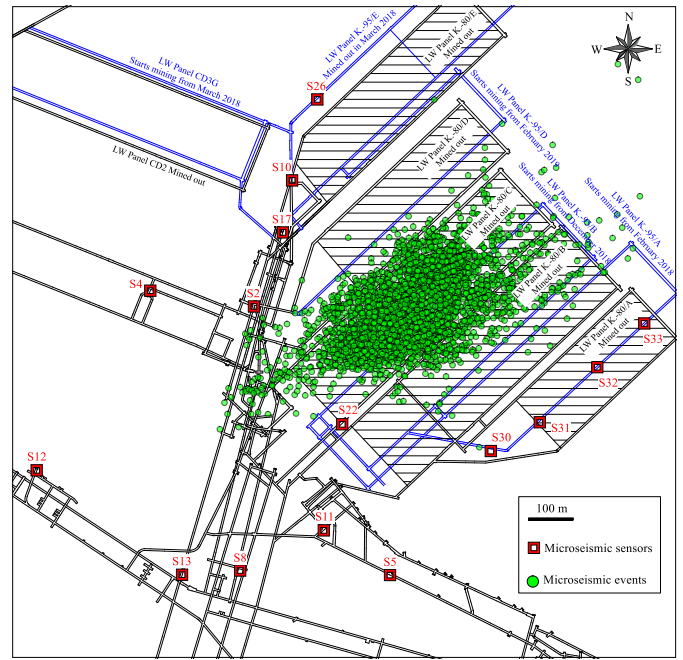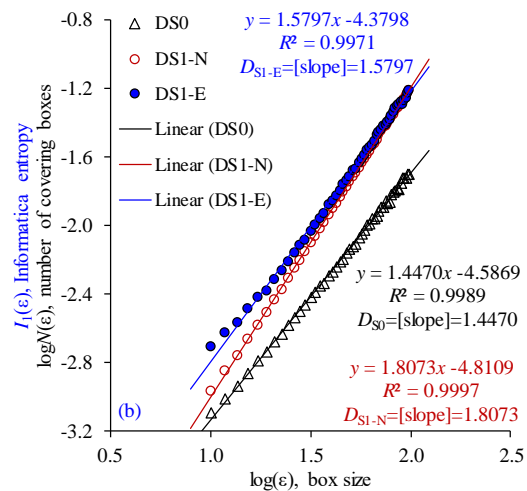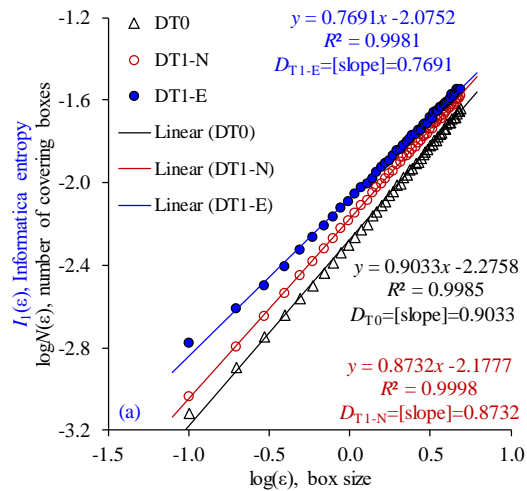
4.2. Model Calibration

During the monitoring period from 01/03/2017 to 01/10/2017, longwall panel K.-80/C was being mined and induced microseismicity mostly clustered in the vicinity and ahead of the advancing longwall face, which makes them to be easily distinguished from other mining activities and thereby to be an appropriate site for the model calibration and its input parameters (weight and background value of each index) determination. Over this period, there were 3,586 microseismic events recorded (see Fig. 8). To calibrate the model, nine fractal dimension based indices (D_{T0}, D_{T1-N}, D_{T1-E}, D_{S0}, D_{S1-N}, D_{S1-E}, D_{E0}, D_{E1-N} and D_{E1-E}) for the whole period were first computed and plotted (Fig. 9). It was found that the correlation coefficients were close to 0.99. This means that the distributions of microseismic events in time, space and energy scales follow a fractal set and the box-counting algorithm adopted in this study is valid.

As illustrated in Fig. 9, the fractal dimensions can be determined through fitting the distribution based on the regression analysis. The values (D_{T0}=0.9033, D_{T1-N}=0.8732, D_{T1-E}=0.7691, D_{S0}=1.4470, D_{S1-N}=1.8073, D_{S1-E}=1.5797, D_{E0}=0.9039, D_{E1-N}=0.9723 and D_{E1-E}=0.9196) were considered as the background values (D_b) of fractal dimensions for seismic hazards assessment over the coming mining period.

Fig. 8. Spatial distribution of microseismic events during LW K.-80/C mining over the period in 01/03/2017-01/10/2017.

$$y = 0.7691x - 2.0752$$
$$R^2 = 0.9981$$
$$D_{T1-E}=[slope]=0.7691$$

$$y = 0.9033x - 2.2758$$
$$R^2 = 0.9985$$
$$D_{T0}=[slope]=0.9033$$

$$y = 0.8732x - 2.1777$$
$$R^2 = 0.9998$$
$$D_{T1-N}=[slope]=0.8732$$

$$y = 1.5797x - 4.3798$$
$$R^2 = 0.9971$$
$$D_{S1-E}=[slope]=1.5797$$

$$y = 1.4470x - 4.5869$$
$$R^2 = 0.9989$$
$$D_{S0}=[slope]=1.4470$$

$$y = 1.8073x - 4.8109$$
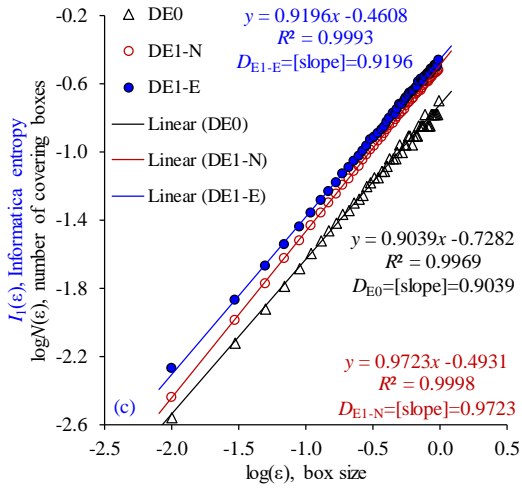$$R^2 = 0.9997$$
$$D_{S1-N}=[slope]=1.8073$$

Fig. 9. Calibration of the fractal dimension based indices using historical microseismic data over the mining period of longwall panel K.-80/C between 01/03/2017 and 01/10/2017.

In order to determine the weighting of each fractal index, the time-sequence curves of fractal indices were first plotted using a time sliding window of ten days and a time sliding step of one day, as an example of D_{S1-E} displayed in Fig. 10. For further details of the calculation process of the time sliding method, please refer to Cai et al. (2018). The figure shows that most of the strong seismic events occurred when the fractal index decreased dramatically and then reached to the low value, which agrees well with the fractal dimensions evolution of tested coal sample under loading to the failure (see Fig. 4). It should be noted that the seismic hazard level will be higher as the energy of seismic event is larger. This also means that the seismic hazard will be more likely to occur.
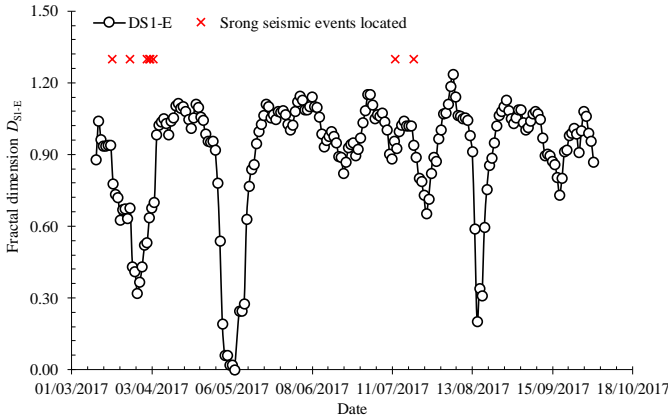

Fig. 10. An example time-sequence of fractal index D_{S1-E}.

Subsequently, the time-sequence values of each fractal index were converted into anomaly index values using Eq. (7). Based on this anomaly index, the F score value of each fractal index was then computed using Eq. (8). After obtaining the F score values of all fractal indices, the weighting of each fractal index was finally calculated using Eqs. (9) and (10), as summarised in Table 1. It should be noted that the basis here for judging whether an assessment is accurate or not is to check whether or not a strong seismic event occurs with the following three days (this time length can be adjusted based on filed-specific conditions) after indices exceed corresponding critical hazards levels (weak, moderate and strong). If the seismic hazard occurs, it is defined as true positive; otherwise, it is false positive. It can be found from Table 1 that D_{S1-E} and D_{E1-E} have a good performance for the assessment of seismic hazards, but others (D_{T1-E}, D_{S0} and D_{S1-N}) have not or even some of them (D_{T0}, D_{T1-N}, D_{E0} and D_{E1-N}) yield in invalid for this case.

Table 1. F score value and weight of each fractal index.

Fractal index	F score	Weighting
D_{T0}	0.0000	0.0000
D_{T1-N}	0.0000	0.0000
D_{T1-E}	0.0321	0.1192
D_{S0}	0.0134	0.0497
D_{S1-N}	0.0158	0.0586
D_{S1-E}	0.1040	0.3860
D_{E0}	0.0000	0.0000
D_{E1-N}	0.0000	0.0000
D_{E1-E}	0.1041	0.3864

4.3. Model Validation

As mentioned in Section 4.1 and confirmed through numerical modelling, longwall gateroad developments in zones of high stress concentration in a new production level (such as moving from level -80 m to -95 m level) often face high risk of seismic hazards. Fig. 11 presents one such stress analysis carried out in FLAC[3D] to establish the peak stress zone ahead of gateroad development for longwall panel K.-95/D, which was being driven below the mined-out panel K.-80/D.

Numerical modelling has clearly shown that driving a heading through the stress abutment zone within the central pillar poses a seismic hazard. As shown in Fig. 7, during the period when longwall panel K.-95/D gateroad was being driven, a spatial clustering (marked with a rectangle) of the events around the region where the gateroad was located can be easily identified. Fig. 12 presents the results of a risk assessment study performed using the spatially smoothed seismicity model (Frankel. 1995; Cai et al., 2015) based on the number of seismic events per m² in the study area. This aimed at identifying potential seismic hazard zones during the period 18/02/2018 to 18/04/2018. It was observed that three potential seismic hazard zones were close to the central pillarand located over/under the barrier pillars of the longwall panels K.-80/E, K.-80/D and K.-80/C.
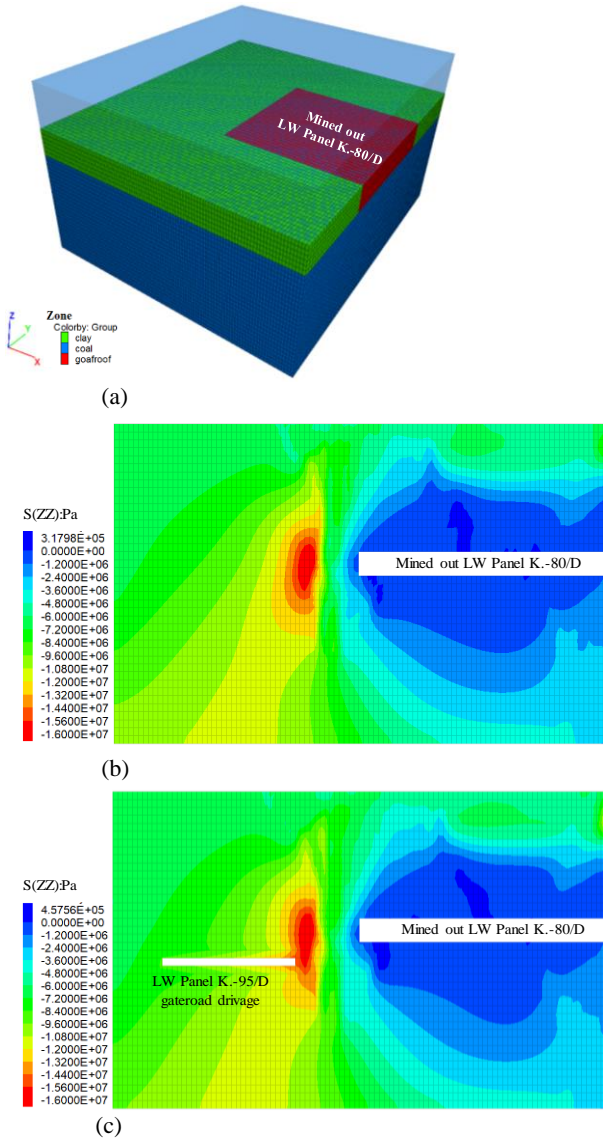
(a)

(b)

(c)

Fig. 11. (a) 3D model geometry and geological representation of the area around longwall panel K.-80/D and stress distribution (b) before and (c) after the longwall K.-95/D gateroad is developed.

Fig.13 presents risk analysis based on temporal evolution of fractal dimension based indices due mainly to driving the gateroad heading for longwall panel K.-95/D. The figure illustrates that there are two periods of dramatic drop to a low value and then an initial increase, suggesting potential seismic hazards. By further processing of these fractal indices utilising the fractal-fuzzy model, a probabilistic assessment for each seismic hazard level and its comprehensive assessment can be achieved (Fig.14). The figure demonstrates a quantitative analysis for the assessment of seismic hazard risk. Such analysis can be conducted on a daily basis and help plan safety measures.
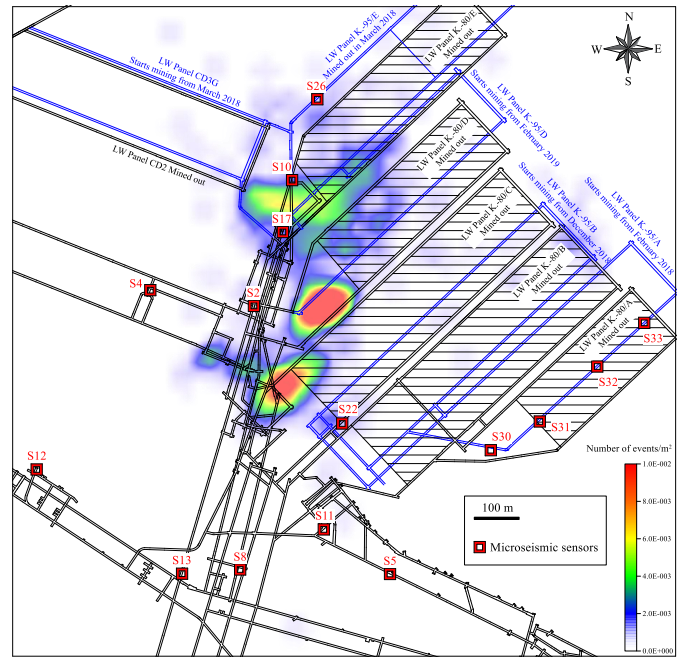

Fig. 12. Hazard assessment based on the density distribution of seismic events recorded in the period 18/02/2018 to 18/04/2018.
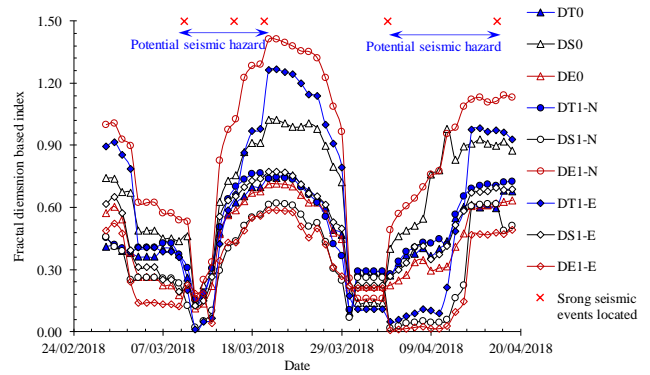

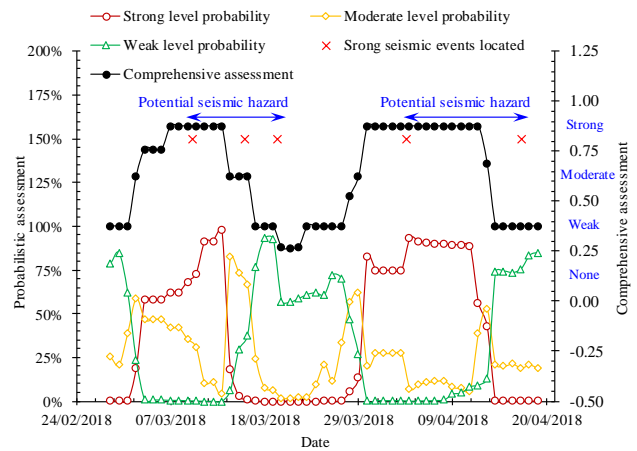Fig. 13. Sequential evolution of fractal indices.

Fig. 14. Probabilistic and comprehensive assessment of seismic hazards.

5. CONCLUSIONS

A methodology for seismic hazards assessment, involving fractal dimension-based indices and fuzzy comprehensive evaluation model, has been developed based on the processed real time microseismic data from an underground coal mine, which allows for a better and quantitative assessment of the likelihood for seismic hazards on a daily basis.

In this methodology, the fractal dimension-based indices used include nine indices in total, from capacity and information dimensions. The membership function in the fuzzy model was built using a Gaussian distribution. The weighting of each index was determined using the performance metric F score derived from the confusion matrix. The assessment results were initially characterised as a probability belonging to each of four risk levels, and on this basis the comprehensive result was then achieved by integrating the maximum membership degree principle (MMDP) and the variable fuzzy pattern recognition (VFPR). The application of this methodology has been successfully demonstrated at Coal Mine Velenje.

REFERENCES

Adoko, A. C., Gokceoglu, C., Wu, L. and Zuo, Q. J., 2013. Knowledge-based and data-driven fuzzy modeling for rockburst prediction. *Int. J. Rock Mech. Min. Sci.* 61, 86-95.

Afraei, S., Shahriar, K. and Madani, S. H., 2018. Statistical assessment of rock burst potential and contributions of considered predictor variables in the task. *Tunn. Undergr. Sp. Tech.* 72, 250-271.

Afraei, S., Shahriar, K. and Madani, S. H., 2019. Developing intelligent classification models for rock burst prediction after recognizing significant predictor variables, Section 1: Literature review and data preprocessing procedure. *Tunn. Undergr. Sp. Tech.* 83, 324-353.

Alber, M., Fritschen, R., Bischoff, M. and Meier, T., 2009. Rock mechanical investigations of seismic events in a deep longwall coal mine. *Int. J. Rock Mech. Min. Sci.* 46(2), 408-420.

Amitrano, D., 2012. Variability in the power-law distributions of rupture events. *Eur. Phys. J.-Spec. Top.* 205(1), 199-215.

Cai, W., Dou, L., Si, G., Cao, A., He, J. and Liu, S., 2016. A principal component analysis/fuzzy comprehensive evaluation model for coal burst liability assessment. *Int. J. Rock Mech. Min. Sci.* (81), 62-69.

Cai, W., Dou, L., Zhang, M., Cao, W., Shi, J. Q. and Feng, L., 2018. A fuzzy comprehensive evaluation methodology for rock burst forecasting using microseismic monitoring. *Tunn. Undergr. Sp. Tech.* 80, 232-245.

Cheng, G., Ma, T., Tang, C., Liu, H. and Wang, S., 2017. A zoning model for coal mining-induced strata movement based on microseismic monitoring. *Int. J. Rock Mech. Min. Sci.* 94, 123-138.

Ding, Y., Dou, L., Cai, W., Chen, J., Kong, Y., Su, Z. and Li, Z. (2016). Signal characteristics of coal and rock dynamics with micro-seismic monitoring technique. *Int. J. Min. Sci. Technol.* 26(4), 683-690.

Fawcett, T., 2006. An introduction to ROC analysis. *Pattern Recogn. Lett.* 27(8), 861-874.

Feng, X. T., Yu, Y., Feng, G. L., Xiao, Y. X., Chen, B. R. and Jiang, Q., 2016. Fractal behaviour of the microseismic energy associated with immediate rockbursts in deep, hard rock tunnels. *Tunn. Undergr. Sp. Tech.* 51, 98-107.

Frankel, A., 1995. Mapping seismic hazard in the central and eastern United States. *Seismol. Res. Lett.* 66(4), 8-21.

Kornowski, J. and Kurzeja, J., 2012. Prediction of rockburst probability given seismic energy and factors defined by the expert method of hazard evaluation (MRG). *Acta Geophys.* 60(2), 472-486.

Li, N. and Jimenez, R., 2018. A logistic regression classifier for long-term probabilistic prediction of rock burst hazard. *Nat. Hazards.* 90(1), 197-215.

Li, T., Cai, M. F. and Cai, M., 2007. A review of mining-induced seismicity in China. *Int. J. Rock Mech. Min. Sci.* 44(8), 1149-1171.

Markič, M. and Sachsenhofer, R.F., 2010. The Velenje lignite - its petrology and genesis. Geological Survey of Slovenia, Ljubljana. ISBN 978-961-6498-20-3.

Mandelbrot, B. B., 1982. *The fractal geometry of nature*. Vol. 1. New York: WH freeman.

Mutke, G., Pierzyna, A. and Baranski, A. 2016. *b*-Value as a criterion for the evaluation of rockburst hazard in coal mines. In *3rd International Symposium on Mine Safety Science and Engineering*, 1-5.

Qian, Q. H., 2014. Definition, mechanism, classification and quantitative forecast model for rockburst and pressure bump. *Rock Soil Mech.* 35(1), 1-6.

Roy, P. N. S. and Gupta, D. K., 2015. Fractal Analyzer: A matlab application for multifractal seismicity analysis. *Seismol. Res. Lett.* 86(5), 1424-1431.

Scholz, C. H., 1968. The frequency-magnitude relation of microfracturing in rock and its relation to earthquakes. *B. Seismol. Soc. Am.* 58(1), 399-415.

Si, G., Durucan, S., Jamnikar, S., Lazar, J., Abraham, K., Korre, A., Shi, J.Q., Zavsek, S., Mutke, G. and Lurka, A., 2015. Seismic monitoring and analysis of excessive gas emissions in heterogeneous coal seams. *Int. J. Coal Geol.*, 149, 41-54.

Sun, J., Wang, L.G., Zhang, H.L. and Shen, Y.F., 2009. Application of fuzzy neural network in predicting the risk of rock burst. *Procedia Earth Planet. Sci.* 1(1), 536-543.

Takuska-Węgrzyn, E., 2008. Application of statistical methods for evaluation of rock-burst risks in copper ore mine conditions. *Arch. Min. Sci.* 53(1), 23-30.

Wang, C., Wu, A., Lu, H., Bao, T. and Liu, X., 2015. Predicting rockburst tendency based on fuzzy matter–element model. *Int. J. Rock Mech. Min. Sci.* 75, 224-232.

Wesseloo, J., 2018. The spatial assessment of the current seismic hazard state for hard rock underground mines. *Rock Mech. Rock Eng.* 51(6), 1839-1862.

Xie, H. and Pariseau, W.G., 1993. Fractal character and mechanism of rock bursts. *Int. J. Rock Mech. Min. Sci. Geom. Abstr.* 30 (4), 343–350.

Yu, Y., Geng, D. X., Tong, L. H., Zhao, X. S., Diao, X. H. and Huang, L. H., 2018. Time fractal behavior of microseismic events for different intensities of immediate rock bursts. *Int. J. Geomech.* 18(7), 06018016.